JOURNAL OF SPACECRAFT AND ROCKETS
Vol. 46, No. 1, January–February 2009

Stiffening and Mechanical Load Effects on Thermal Buckling of Stiffened Cylindrical Shells

Theodore F. Johnson* and Michael F. Card†
NASA Langley Research Center, Hampton, Virginia 23681-2291

DOI: 10.2514/1.24575

A study of combined thermal and mechanical buckling of stiffened cylindrical shells using the structural geometry of a preliminary supersonic transport fuselage design from 1970 is presented. The buckling analysis is performed using BOSOR4, a nonlinear axisymmetric shell-of-revolution analysis code. The mechanical load is from axial compression and internal pressure and the thermal loading is from heated skins. Results indicate that the location of longitudinal eccentric stiffening has a significant effect on the thermal and axial buckling strength of longitudinally stiffened shells with and without ring frames. Buckling-interaction curves of the results with the associated mode shapes and a surface plot of the results are presented in which the eccentricity of the stringer, axial load, and temperature load are varied.

Nomenclature

A	=	area, in.^{2}
E	=	modulus of elasticity, ksi
e	=	eccentricity of stiffening members, in.
GJ	=	torsional rigidity, lb $\cdot$ in.^{2}
I	=	moment of inertia, in.^{4}
Nx	=	axial line load, lb/in.
T	=	temperature, °F
u, v, w	=	displacement in the x, y, and z directions, in.
$w_{,x}$	=	rotation about the z axis, deg.
α	=	coefficient of thermal expansion, in./in. $\cdot$ °F
ν	=	Poisson's ratio

Subscripts

ext	=	external
int	=	internal

Introduction

AEROSPACE-SYSTEM studies in the 1990s [1–3] indicated a renewal of interest in supersonic transports (SSTs) and single-stage-to-orbit (SSTO) reusable launch vehicles (RLVs). Because of the moderate-to-high heating rates, both vehicles experienced thermal stresses caused by temperature differences between the skin and stiffening members. If the primary structures were large stiffened shells, the designer had to ensure that the structure would not buckle under anticipated temperature increases.

The effects of stiffening, thermal loads, and axial compression were presented by Chang and Card [4] with thermal loading from heated skins, but they did not investigate the effect of boundary conditions or show buckling-mode shapes as the loading changed. However, the stress states in the axial and circumferential directions were documented. Kossira and Haupt [5] studied thermal buckling in plates and shells and calculated half-mode shapes. The thermal load, however, was for local strip heating only. Thermal buckling in orthotropic cylindrical shells was studied by Radhamohan and Venkataramana [6]. They used Sander's equations to determine the buckling response. The boundary conditions such as the axial displacement and inclusion of the prebuckling rotations at the shell ends in the Radhamohan and Venkataramana analyses had a significant effect on the critical buckling temperature. A comprehensive review of thermal buckling in plates and shells by Thorton [7] indicated that research on the thermal effect of buckling in metallic plates and shells was on the decline, whereas studies on thermal buckling in orthotropic structures was increasing. However, the number of laboratory tests to verify the analytical portion of these studies had reduced significantly. Eslami et al. [8] produced a significant number of contributions to the study of thermal buckling of shells using modified Donnell equations. The temperature effects related to creep [9] and imperfections [10] on thin stiffened cylindrical shells were investigated in the Eslami et al. [8] studies. However, buckling studies of cylindrical shells that include the effects of structural geometry, axial load, and thermal load have not been performed since Chang and Card [4] or until this paper.

The predicted buckling behavior of generic stiffened cylindrical shells with a finite length and subjected to a combination of mechanical and thermal loading is investigated in this paper through analysis. The objective of this paper is to extend the work of Chang and Card [4] and to further study the effects of the boundary conditions and eccentricity of longitudinal stiffeners on the buckling behavior of cylindrical shells. To restrict the number of computations, the shell is limited to a finite length for which general instability is infeasible and buckling interaction is between the bounds of panel instability (from mechanical loads) and local instability (from circumferential thermal stresses at the ends due to end restraints). The relationship between thermal buckling and buckling due to axial loading is presented. The three models used in the study are a stiffened cylinder with ring frames, a stiffened cylinder without ring frames, and a periodic model with a ring frame and stiffeners. These three models are used in this paper to investigate the influence of the number of ring frames, longitudinal stiffeners, and boundary conditions on the buckling behavior of cylindrical shells.

Approach

A brief description of the analysis code and how the analysis code was employed in the study is provided. The models, boundary conditions, and rationale for the applied loading are described in this section. The results from the analyses are presented and discussed in the subsequent section.

Presented as Paper 1317 at the 36th AIAA/ASME/ASCE/AHS/ASL Structures, Structural Dynamics, and Materials Conference, New Orleans, LA, 10–12 April 1995; received 11 April 2006; accepted for publication 19 July 2006.

*Aerospace Engineer, Mechanics of Structures and Materials Branch, Mail Stop 431; Theodore.F.Johnson@nasa.gov. Member AIAA.
†Chief Scientist. Fellow AIAA.

Analysis Code

A nonlinear finite difference shell-of-revolution code, BOSOR4 [11], is used as the analysis tool in this study. BOSOR4 is based upon the Vlasov–Sanders shell theory and is used to conduct both nonlinear prebuckling and buckling analyses [12] for all cases presented herein. BOSOR4 uses modal iteration to determine eigenvalues. The code is efficient for developing buckling-interaction curves, but for the models analyzed in this paper, the solution algorithm (modal iteration) is sensitive to the initial eigenvalue and eigenvector, because the eccentricity of the stringer is varied. Multiple solutions occur along some points of the interaction curves. The previous solution is used as an initial point for the next analysis to direct the analyses along a feasible solution path.

Model

The structural configuration is adapted from an early (1970) SST design, shown in Fig. 1 [13]. The SST was a proposed commercial vehicle with delta wings that would cruise at Mach 2. The fuselage structure is simplified to an axisymmetric shell of revolution without imperfections, as shown in Fig. 2 [4]. The three models in this study used the material properties in Table 1 [4].

The shell is modeled with at least six nodes per inch along the shell length to ensure that local instability modes are captured. Ring frames are modeled as discrete beams, and the stiffness of the stringers is smeared into the skin properties in the first two models. Thus, ring-frame and stringer crippling, or rollover, cannot be investigated with these two models. In the third model, the ring frame is modeled discretely to investigate ring-frame crippling. The stringers, however, are also smeared into the skin. Eccentricity is measured from the centroid of the stiffening member to the reference surface of the shell, as shown in Fig. 3.

Boundary Conditions

Simple-support boundary conditions represent the bulkheads at each end of the shell. The coordinate system of the shell model is shown in Fig. 3. The shell is allowed to grow axially in the x direction at both ends, but is constrained from expanding in the radial direction or z direction. The ends are allowed to move axially so that axial line loads Nx can be introduced into the shell. Rotations $w_{,x}$ at the ends are permitted because the skin is considered to be extremely flexible, compared with the bulkheads. Axial motion at the center longitudinal plane of the shell is restricted to eliminate rigid-body motion in the longitudinal direction.

A complete list of the boundary conditions used in the analysis is presented in Tables 2–4. The boundary conditions for studies of longitudinally stiffened shells without ring frames in which symmetry is employed at one end of the shell are listed in Table 2. The boundary conditions for full-length shells with ring frames and stringers are listed in Table 3. The boundary conditions are prescribed at three points for full-length shells. The ends are allowed to be free so that an axial load Nx can be introduced in the prebuckling phase of the analysis. Fixing the displacement in the x direction at the center prevents rigid-body motion of the shell. Once the shell begins to buckle, an additional boundary condition, fixing displacement v in the tangential direction, must be applied to obtain a feasible solution. The boundary conditions in Table 4 (symmetry is employed at both ends) simulate an infinitely long cylindrical shell as a periodic shell model. The periodic shell model enables the study of the behavior of the interior structural members of a shell, such as a ring frame.

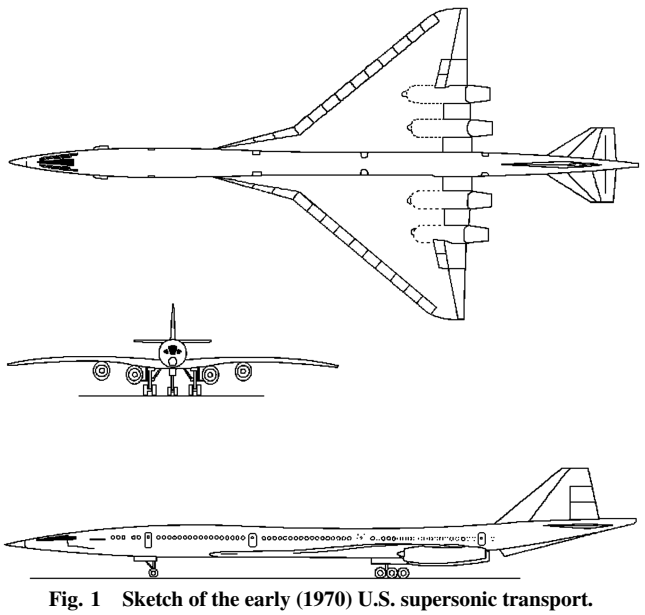

Fig. 1 Sketch of the early (1970) U.S. supersonic transport.

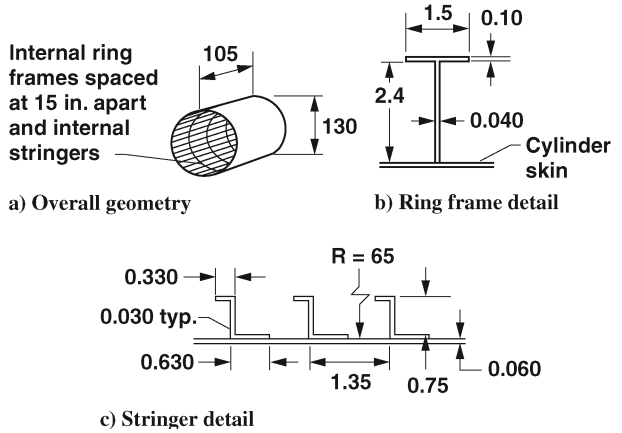

Fig. 2 Geometry of the a) cylindrical shell, b) typical ring frame, and c) stringer-stiffened shell with internal stringers; dimensions are in inches.

Loading

The skin of the shell is loaded with a uniform axial line load, a uniform temperature change on the skin, and internal pressure. The axial line loads are applied at the two ends in opposing directions on the centroid of the shell and stringer cross section. The uniformly distributed axial line load represents an approximation to the maximum load due to bending of the fuselage.

A uniform temperature change is applied only to the skin, as in [4]. The temperature change is not applied to the ring frames, stiffeners, or bulkheads. No temperature change is applied to the skin where the bulkheads and ring frames come into contact with the skin; as a result, a temperature gradient is formed in the axial direction. The described temperature loading occurs as the vehicle climbs to altitude. As an SST-type vehicle ascends, the outside temperature rises, whereas the internal stiffeners and bulkheads remain cool. The difference is due to the thermal mass of the members and the climate conditions inside the cabin. The internal cabin pressure of the vehicle dictates the pressure applied to the shell.

Table 1 Material properties and geometry of members of an internally stiffened shell

		Member		
Property	Unit	Skin	Ring frame	Stringer
E	ksi	14.5×10^3	16.4×10^3	16.4×10^3
ν	——	0.30	——	——
α	in./in. · °F	5.0×10^{-5}	——	——
A	in.^{2}	——	0.246	0.0495
I	in.^{4}	——	0.1377	0.004083
GJ	lb · in.^{2}	——	3477	0.000
e	in.	——	−1.992	−0.342 to 0.342

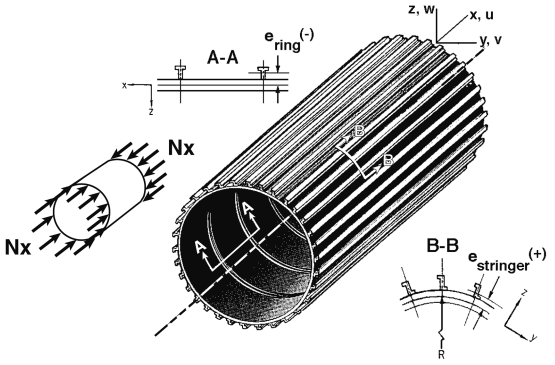

Fig. 3 Coordinate system of an externally stiffened shell model, placement of axial loads, and depiction of stiffeners eccentricities.

Results and Discussion

The results presented herein are in the form of tables, buckling-interaction curves, and a surface plot with axial and temperature loads as parameters. The influence of the number of ring frames is presented to illustrate how global instabilities are avoided. A surface plot is presented for the cases in which the following parameters are varied: axial load, temperature load, eccentricity, and internal pressure. Finally, the results for models with and without end effects are presented to demonstrate the effect of boundary conditions.

Two distinct buckling modes were generated from the analyses that had a direct influence on the shape of the buckling-interaction curves. Ross et al. [14] showed that when a shell buckles due to thermal loads, local instability at the boundaries leads to buckling. Local instability occurs when the boundaries are rigid compared with the shell, and it causes high circumferential stress. Panel instability is usually associated with axial loading or end shortening [15].

Table 2 Prebuckling and buckling boundary conditions for interior shell models employing symmetry at one end

	Left end	Right end (plane of symmetry)
u	Free	Fixed
v	Fixed	Free
w	Fixed	Free
$w_{,x}$	Fixed	Fixed

Table 3 Boundary conditions for a full-length ring-frame- and stringer-stiffened shell

	Left end	Center	Right end
Prebuckling			
u	Free	Fixed	Free
v	Fixed	Free	Fixed
w	Fixed	Free	Fixed
$w_{,x}$	Free	Free	Free
Buckling			
u	Free	Fixed	Free
v	Fixed	Free	Fixed
w	Fixed	Free	Fixed
$w_{,x}$	Free	Free	Free

Table 4 Prebuckling and buckling boundary conditions for single-ring-frame models employing symmetry at both ends

	Left end	Right end
u	Free	Fixed
v	Fixed	Free
w	Free	Free
$w_{,x}$	Fixed	Fixed

Influence of Length and Ring-Frame Effects

The impact of the length of the shell and of the number of ring frames on axial or thermal buckling results is investigated by comparing the buckling results for models with three-, four-, five-, or six-ring frames. The axial or thermal buckling load versus the number of ring frames is shown in Fig. 4 with the wave number for each solution. There is a small change in wave number and no significant difference in temperature or axial buckling load. When considering four or more ring frames, the results do not vary for either temperature loading or axial loading. The buckling load for axial loading is 2800 ± 10 lb/in. Buckling due to thermal loading occurs at $580 \pm 2°$F. The wave numbers for models with three- to six-ring frames with axial loading are 51 and 52, and for models with thermal loading, the wave numbers are 61 and 62.

The results in Fig. 4 indicate that the addition of ring frames would not result in a more accurate solution. A six-ring-frame model is used to represent a complete shell for all subsequent studies. The restriction of the shell to a length of six-ring frames eliminates general instability (the ring frame deflects with the skin) as a buckling mode in the present studies. Thus, the buckling interaction investigated herein varies between panel instability from axial compression and local buckling from circumferential stress due to end constraints and temperature change.

Longitudinally Stiffened Shells

The buckling-interaction curves and mode-shape results from the analyses of longitudinally stiffened shells are presented in Figs. 5 and 6. The buckling response of cylindrical shells with longitudinal stiffeners that are located either on the internal or external surface are investigated. The results are for the models with the geometries shown in Figs. 2 and 3.

No interaction between panel buckling modes and local buckling modes is seen for cylindrical shells with longitudinal stiffeners, as shown in Figs. 5 and 6. The buckling modes are separate, with no simple transition between the modes. The shell buckles due to panel instability in the portion of the buckling-interaction curve with circular symbols, and it buckles due to local instability in the portion of the curve with square symbols in Figs. 5 and 6. Panel instability is due to axial load, whereas local instability is due to high circumferential stresses caused by the imposed temperature change and end constraints. The half-mode shape (symmetry is employed) for each type of buckling is indicated on the figures. The maximum peaks on the mode-shape plots indicate the location at which the shell will buckle.

The buckling results for an internally stiffened shell subjected to thermal load, shown in Fig. 5, indicate that the shell can tolerate a temperature change of almost three times the temperature change

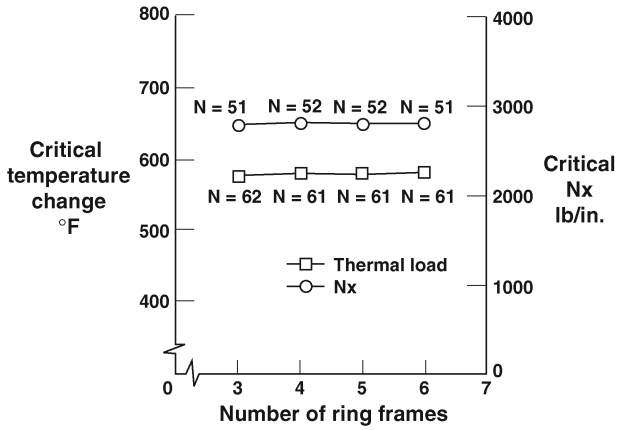

Fig. 4 Effect of the number of ring frames on the critical buckling temperature and critical axial load.

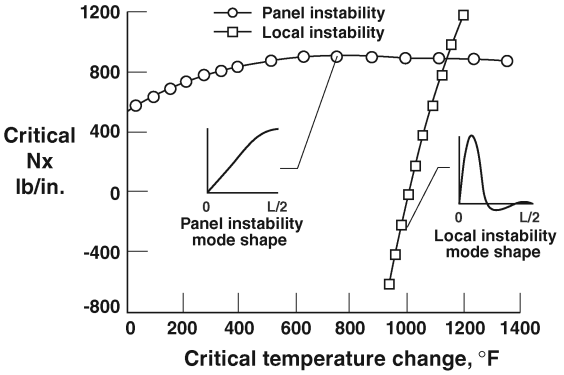

Fig. 5 Buckling-interaction curve and associated half-mode shapes for a shell with stringers that have an eccentricity of −0.342 in. (internal) and no-ring frames.

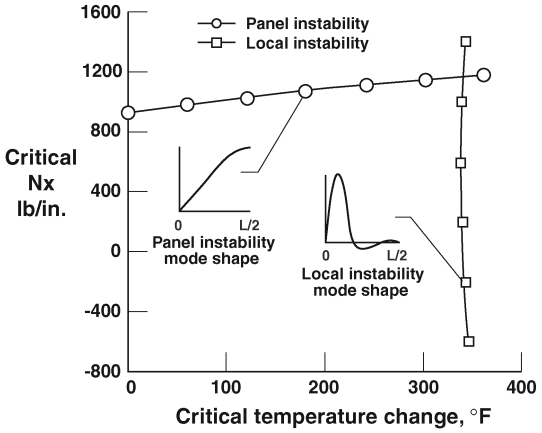

Fig. 6 Buckling-interaction curve and associated half-mode shapes for a shell with stringers that have an eccentricity of 0.342 in. (external) and no-ring frames.

withstood by the externally stiffened shell in Fig. 6 ($T_{int} = 1003°F$ vs $T_{ext} = 340°F$). This extreme difference is an inherent benefit for internally stiffened shells subjected to thermal loading. The externally stiffened shell can withstand almost twice the pure axial load carried by the internally stiffened shell ($Nx_{int} = 561$ lb/in. vs $Nx_{ext} = 922$ lb/in.). The latter result is well documented for longitudinally stiffened shells when comparing the relative strength of external stiffening with internal stiffening [15].

Ring-Frame- and Stringer-Stiffened Shells

Stiffened shells with internal ring frames and stringers that are internal or external are investigated in this section. The buckling-interaction curve for a ring-frame- and stringer-stiffened shell with internal longitudinal stringers with an eccentricity of −0.342 in. is shown in Fig. 7. The critical temperature, critical axial load, and circumferential wave number are listed in Table 5.

During the initial generation of the data to plot the buckling-interaction curve shown in Fig. 7, the axial load was the eigenvalue parameter used in BOSOR4. Because multiple solutions could exist beyond the portion of the curve dominated by axial load, temperature was used as the eigenvalue parameter. Any solution that is not under the buckling-interaction curve is not a feasible solution because the shell will buckle from either axial or thermal load.

The buckling-interaction curve shown in Fig. 7 has a similar shape when compared with the curve produced by Chang and Card [4] in Fig. 8. The Chang and Card results were different because Chang and Card used their own analysis code based on the Donnell equations. Three distinct buckling modes are present in the buckling-interaction curve presented in Fig. 7. All of the buckling modes significantly influence the shape of the curve. The shell buckles from axial load

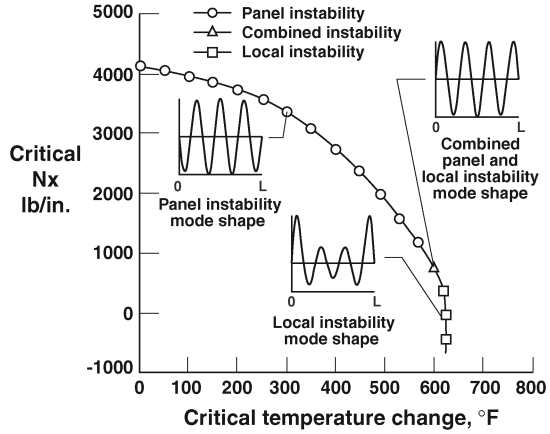

Fig. 7 Buckling-interaction curve and associated mode shapes for a shell with internal ring frames and stringers that have an eccentricity of −0.342 in. (internal).

(i.e., panel instability) in the portion of the curve with circular symbols. The associated mode shape is indicated in Fig. 7. Axial buckling is caused by axial load that causes high stresses in the axial direction of the shell and skin dimpling. In the portion of the curve with square symbols, buckling is caused by thermal load or local instability. Buckling due to thermal load only is induced by high circumferential stresses developed in the skin at the cool bulkheads (edge effect). In the center portion of the curve (portion with triangular symbols), the two mode shapes interact with each other, forming a third mode shape (hybrid or combined mode shape).

The wave numbers shown in Table 5 decrease as the axial load changes from tension to compression (compression is positive). The

Table 5 Buckling results for an internally stiffened shell with ring frames and pressure of 0.0 psi

Instability mode	Critical temperature, °F	Critical axial load Nx, lb/in.	Circumferential wave number
Local	0	4122	23
	25	4083	23
	50.01	4043	23
	75	4000	24
	99.99	3956	24
	125	3905	25
	150	3853	26
	175	3797	27
	200	3734	28
	225	3664	30
	250	3580	32
	275	3486	34
	300	3376	37
	324.9	3249	39
	350.1	3102	42
	375	2942	44
	399.9	2765	46
	421.3	2600	47
	446	2400	49
	469.1	2200	51
	490.8	2000	52
	511.4	1800	53
	530.8	1600	54
	549.3	1400	55
	566.6	1200	56
Hybrid	583.9	1000	57
	598.3	800	58
	610.3	600	59
Panel	619.2	400	60
	624.2	200	62
	626.5	0	63
	624.5	−200	65
	623.9	−400	66
	623.5	−600	67

instability modes are also indicated in Table 5. This trend indicates that the mode shapes change along the curve in Fig. 7 in a smooth transition. The mode shape quickly changes from panel instability to the hybrid mode shape at the change in shape of the curve as the curve is traversed from above. However, there is a smooth transition from local instability to the hybrid mode shape as the buckling-interaction curve is traversed from below.

The buckling results for a shell in which the centroid of the stringers is located at the reference surface or midplane (eccentricity is 0.000 in.) of the shell are shown in Fig. 9. The three distinct mode shapes are also indicated on the plot. On the portion of the curve on which panel instability is the dominant buckling mode, the curve slopes downward at a steeper angle than the same portion of the curve in Fig. 7. The local instability portion of the curve is more inclined toward the *y* axis than in the plot in Fig. 7.

The buckling results for a shell with longitudinal stiffeners external to the shell at an eccentricity of 0.342 in. are shown in Fig. 10. The portion of the curve in which the hybrid instability mode is the dominant buckling mode has a larger portion of the curve than in the plots in Figs. 7 and 9. The panel instability portion of the curve slopes at a faster rate than the curves in Figs. 7 and 9, whereas the local instability portion slopes further inward toward the *y* axis than the local instability portion of the curves in Figs. 7 and 9.

The effects of changing the eccentricity of the stringers is shown in Figs. 7, 9, and 10 to illustrate how the shape of the buckling-interaction curve develops a large hump as the centroid of the longitudinal stiffeners is moved through the thickness of the shell. This distortion occurs where hybrid instability modes are located. The buckling modes observed in the results remain the same in Figs. 7, 9, and 10, but the shape of the buckling-interaction curve varies with the eccentricity. The change in shape of the buckling-interaction curve is most pronounced when the longitudinal stiffeners are fully external to shell.

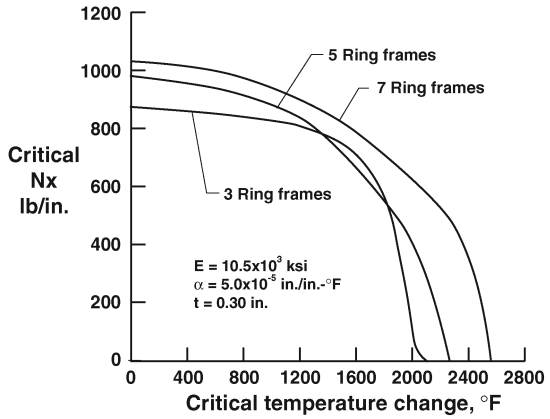

Fig. 8 Buckling-interaction curves from Chang and Card [4].

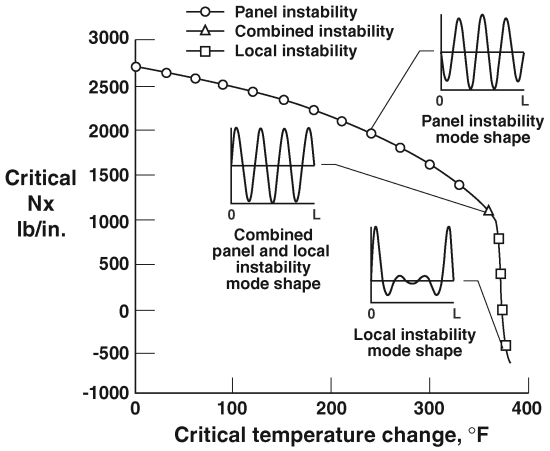

Fig. 9 Buckling-interaction curve and associated mode shapes for a shell with internal ring frames and stringers that have an eccentricity of 0.000 in. (midplane).

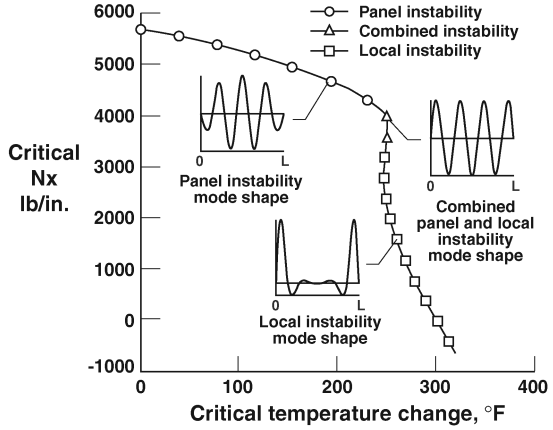

Fig. 10 Buckling-interaction curve and associated mode shapes for a shell with internal ring frames and stringers that have an eccentricity of 0.342 in. (external).

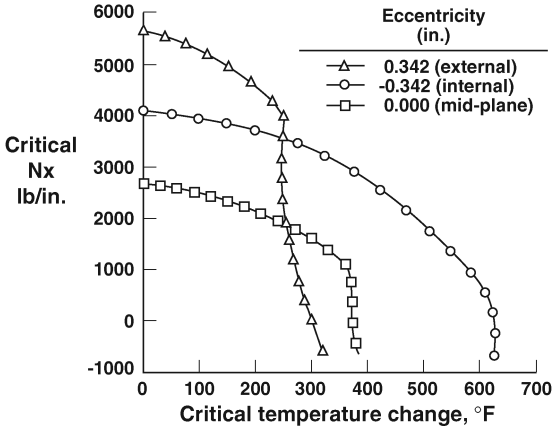

Fig. 11 Buckling-interaction curves for shells with internal ring frames and stringers at three eccentricities.

The dramatic effect of changing the stiffener eccentricities can be seen in Fig. 11, in which the buckling-interaction curves for the three eccentricities (internal, midplane, and external) is superimposed on one plot. As the centroid of the stringers passes through the midplane of the shell wall (internal to external), the axial buckling load decreases then increases, but the thermal buckling load decreases. The increase in eccentricity increases the axial buckling load. The axial load increases by 1.4 times ($Nx_{int} = 4122$ lb/in. vs $Nx_{ext} = 5568$ lb/in.) at the two extremes for longitudinal stiffening. The thermal buckling load increases by over two times ($T_{int} = 626°F$ vs $T_{Ext.} = 300°F$) as the eccentricity changes from internal to external stiffening with no axial load.

The buckling results are also depicted in a three-dimensional surface plot in Fig. 12, in which the buckling-interaction surface distorts as the eccentricity of the longitudinal stringer, temperature load, and axial load are varied at an internal pressure of 0.0 psig. The reduction in buckling temperature and parabolic variation in the buckling axial load as the eccentricity varies from an internal to external location can be seen in Fig. 12. The results in the surface plot indicate that as the centroid of the stringers is moved closer to the reference surface, not only does the ability of the shell to resist thermal load decrease, but so does the ability of the shell to withstand axial load.

An additional two buckling-interaction surface plots were computed with internal pressures of 4.0 and 8.0 psig. The family of surface plots indicates that the temperature and axial load values increase with pressure, but the overall characteristic shape of the results in the surface plots remained the same. These results agreed

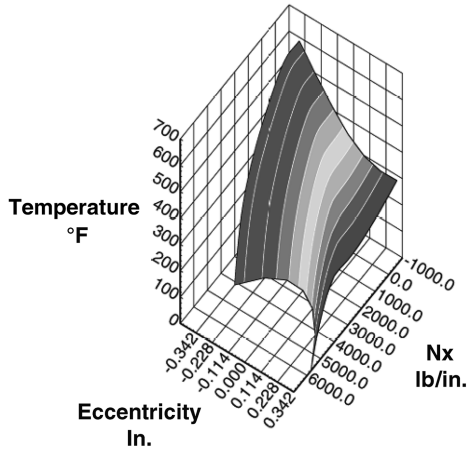

Fig. 12 Buckling-interaction surface for a cylinder with internal ring frames and stringers that have various eccentricities.

with the Brush and Almroth [16] theory that as the internal pressure increases, the stability of the shell increases.

Effects of Boundary Conditions

Boundary conditions can significantly affect the response of a stiffened shell [14,15]. A ring-frame section, or repeating-bay model of a ring frame with a stringer-stiffened shell wall, is created with only a single-ring frame. A plot of the model in its undeformed and deformed shape is presented in Fig. 13. Two models are created to investigate the behavior of the ring-frame or internal section of the shell away from edge effects when loaded with mechanical and thermal loads. One model has internal stiffening and the other has external stiffening. The symmetry boundary conditions at each end of the models are listed in Table 4. The right end is allowed to move axially to introduce the axial load into the shell, whereas the left end is restrained in the axial direction. The buckling-interaction curves for cylindrical shells with internal and external stiffeners are shown in Fig. 14. The results from the full-length model and the single-ring-frame model are compared in Table 6.

Fixed boundary conditions at both of the ends have a significant effect on the buckling behavior of the shells. When loaded under pure axial compression, the results plotted in Fig. 14 show that the externally stiffened shell can carry a greater load than the internally stiffened shell (Nx_{int}3816 lb/in. vs $Nx_{\text{ext}} = 4972$ lb/in.), but when loaded under a pure temperature load, the internally and externally stiffened shell can support a similar amount of temperature change ($T_{\text{int}} = 486$°F vs $T_{\text{ext}} = 499$°F). The ring frame is much stiffer than the skin, such that the ring frame does not move as the skin buckles. The fixed ends result in two of the models with the same mode shapes

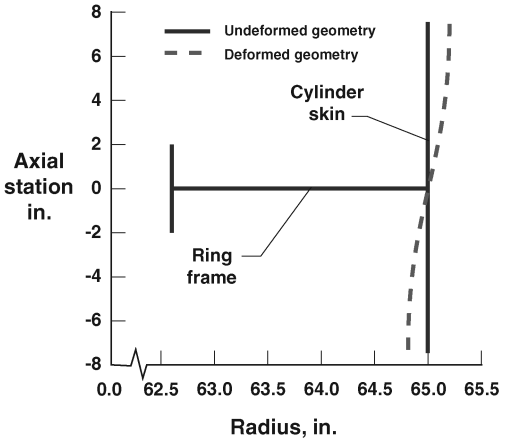

Fig. 13 Mode shape (panel instability) for a stiffened single-ring-frame model (repeating element model) with either internal or external stringers that have eccentricity of ±0.342 in.

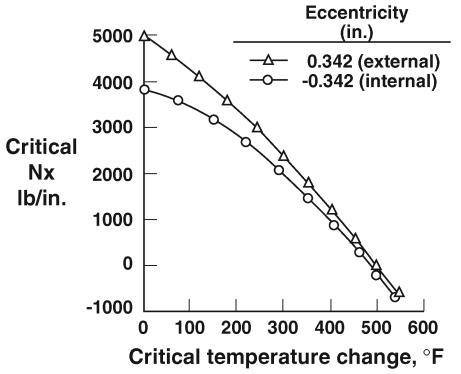

Fig. 14 Buckling-interaction curves for a stiffened single internal ring-frame model (repeating element model) with either internal or external longitudinal stiffening at eccentricities of ±0.342 in.

along the entire buckling-interaction curve in Fig. 14. The shapes of the buckling-interaction curves are similar and actually converge as the temperature increases.

The buckling results for the single-ring-frame models and the full-length models, as shown in Table 6, suggest that models under pure axial load are less dependent on the boundary conditions than models under pure thermal load, but they are still affected. However, a comparison of the thermal buckling results indicates that the boundary conditions play a critical role in the calculation of the buckling temperature load. The thermal buckling load decreases for the internally stiffened shell and substantially increases for the externally stiffened shell.

Conclusions

A numerical study of the buckling behavior of a generic stiffened shell for a representation of an SST is presented. Longitudinally stiffened shells with and without ring frames are considered in this study using three models. Analysis of buckling under combined mechanical load and thermal load is conducted using BOSOR4, a finite difference shell-of-revolution code. The combined thermal and mechanical buckling analysis corresponds to a situation when the shell or skin is heated, but the ring frames, stringers, and ends of the shell remain cool while a mechanical axial load is applied.

Results for the shell with longitudinal stiffening and no-ring frames indicate a significant difference in buckling response due to the eccentric positioning of the longitudinal stiffeners. Buckling results indicate that under pure thermal load, internal longitudinally stiffened shells withstand a critical buckling temperature change of almost three times that of externally stiffened shells. The opposite trend occurs when there is only mechanical loading. An internally stiffened shell carries approximately half the axial compressive load carried by the externally stiffened shell before buckling.

Under pure thermal loading, the internal longitudinal stiffened shell withstands twice the temperature change of the comparable shell with external longitudinal stiffening. The shells with external longitudinal stiffeners withstand a greater mechanical load than shells with internal stringers and ring frames. Additional studies of the combined effects of internal pressure, axial load, and thermal load indicate that the pressure tends to stabilize the shell, thus increasing the critical axial and thermal load.

Table 6 Comparison of the buckling temperature and axial loads for the three models

Model type	Loading			
	Temperature		Axial	
	Internal	External	Internal	External
No-ring frames	1003	340	561	922
Six-ring frames	626	300	4122	5568
Single-ring frames	486	499	3816	4972

A comparison of the buckling results for stiffened shells with an internal single-ring frame with the results for a stiffened shell with six internal ring frames indicates that for axial compressive loads, the buckling results are similar. These results suggest that the effect of the boundary conditions is not significant for axially loaded cylinders. However, the boundary conditions significantly change the thermal buckling load for both the internally and externally stiffened shells when comparing the single-ring-frame shell with the six-ring-frame shell. The eccentricity effects are different for thermal buckling, with virtually no effect on the single-ring-frame shells when comparing internally longitudinal stiffened shell with an externally longitudinal stiffened shell. As noted by previous investigators, thermal buckling is strongly influenced by boundary conditions. The present paper demonstrates that eccentricity and edge effects influence thermal buckling.

Acknowledgment

The authors express their appreciation to David Bushnell for running some cases and for helpful discussions on the thermal buckling phenomena.

References

[1] "U.S. Supersonic Commercial Aircraft—Assessing NASA's High Speed Research Program," *Committee on High Speed Research, National Research Council*, National Academy Press, Washington, D.C., 1997.

[2] "Access to Space Study Final Report," NASA, July 1993.

[3] Freeman, Jr., D. C., Stanley, D. O., Camarda, C. J., Lepsch, R. A., and Cook, S. A., "Single-Stage-to-Orbit: A Step Closer," 45th Congress of the International Astronautical Federation, International Astronautical Federation Paper 94-V3.534, Oct. 1994.

[4] Chang, L. K., and Card, M. F., "Thermal Buckling Analysis for Stiffened Orthotropic Cylindrical Shells," NASA TN-D-6332, 1971.

[5] Kossira, H., and Haupt, M., "Buckling of Laminated Plates and Cylindrical Shells Subjected to Combined Thermal and Mechanical Loads," *Buckling of Shells Structures, on Land, in the Sea and in the Air*, edited by J. F. Jullien, Elsevier, London, 1991, pp. 201–212.

[6] Radhamohan, S. K., and Venkataramana, J., "Thermal Buckling of Orthotropic Cylindrical Shells," *AIAA Journal*, Vol. 13, No. 3, 1975, pp. 397–399.

[7] Thornton, E. A., "Thermal Buckling of Plates and Shells," *Applied Mechanics Reviews*, Vol. 46, No. 10, 1993, pp. 485–506.

[8] Eslami, M. R., Ziaii, A. R., and Ghorbanpour, A., "Thermoelastic Buckling of Thin Cylindrical Shells Based on Improved Stability Equations," *Journal of Thermal Stresses*, Vol. 19, No. 4, 1996, pp. 299–315.
doi:10.1080/01495739608946177

[9] Eslami, M. R., and Shariyat, M., "Elastic, Plastic, and Creep Buckling of Imperfect Cylinders Under Mechanical and Thermal Loading," *Journal of Pressure Vessel Technology*, Vol. 119, No. 1, Feb. 1997, pp. 27–36.
doi:10.1115/1.2842263

[10] Eslami, M. R., and Javaheri, R., "Thermal and Mechanical Buckling of Composite Cylindrical Shells," *Journal of Thermal Stresses*, Vol. 22, No. 6, 1999, pp. 527–545.
doi:10.1080/014957399280733

[11] Bushnell, D., *BOSOR4: Program for Stress and Vibration of Shells of Revolution*, edited by N. Perrone, and W. Pilkey, Structural Mechanics Software Series, Vol. 1, Univ. Press of Virginia, Charlottesville, VA, 1977, pp. 11–143.

[12] Bushnell, D., "Stress, Stability and Vibration of Complex Shells of Revolution: Analysis and User's Manual for BOSOR4," NASA CR-2115, Oct. 1972.

[13] Corning, G., *Supersonic and Subsonic Airplane Design*, 3rd ed., 7th Printing, Braun–Brumfield, Ann Arbor, MI, 1970, p. 484.

[14] Ross, B., Hoff, N. J., and Horton, W. H., "The Buckling Behavior of Uniformly Heated Thin Circular Cylindrical Shells," *Monocoque, Sandwich and Composite Aerospace Structures—Selected Papers of Nicholas J. Hoff*, Technomic, Lancaster, PA, 1986, pp. 313–321; also *Experimental Mechanics*, Vol. 6, No. 11, Nov. 1966, pp. 529–537.
doi:10.1007/BF02327232.

[15] Anderson, M. S., "Thermal Buckling of Cylinders," Collected Papers on Instability of Shell Structures, NASA TN-D-1510, 1962, pp. 267–276.

[16] Brush, D. O., and Almroth, B. O., *Buckling of Bars, Plates, and Shells*, McGraw–Hill, New York, 1975.

G. Agnes
Associate Editor